



Characterization of the adherence strength and the aggregate-paste bond of prestressed concrete with siderurgical aggregates

P. Tamayo^a, A. Aghajanian^a, J. Rico^b, J. Setién^a, J.A. Polanco^a, C. Thomas^{a,*}

^a LADICIM (Laboratory of Materials Science and Engineering), Universidad de Cantabria. E.T.S. de Ingenieros de Caminos, Canales y Puertos, Av./ Los Castros 44, 39005, Santander, Spain

^b Construction Engineering, Research and Project Development (INGECID S.L.), E.T.S. de Ingenieros de Caminos, Canales y Puertos, Av./ Los Castros 44, 39005, Santander, Spain

ARTICLE INFO

Keywords:

Adherence
Prestressed concrete
EAFS
Siderurgical aggregates
Hardness
ITZ

ABSTRACT

Concrete with siderurgical aggregates (SA) is a sustainable construction material with great potential as structural concrete. For this reason, studies must be carried out on the behavior of concrete against prestressed elements, studies that open the door to new applications such as buildings, bridges or foundations. In this study, the feasibility of prestressed concrete is established with standardized adherence tests on beams reinforced with steel wires. The comparison between the concrete-reinforcement union of limestone concrete and concrete with siderurgical aggregates, has shown to be 23% higher in the case of the latter. This study is completed with the analysis of the paste-aggregate interface (ITZ) of both types of aggregate to support the results obtained in the adherence test. In addition, in order to know the bond strength of the pastes that incorporate SA, the micro-Vickers hardness of the pastes of the concrete mixes are determined, a hardness that has turned out to be proportional to the replacement of fine aggregates with SA.

1. Introduction

The current policies of the European Union (EU), within the framework of the 2021–2030 strategic plan, promote economic growth through efficiency policies, clean energy, sustainability, and reduction in the use of natural resources. The latter can be applied by obtaining value from waste and by-products which, in the case of concrete (the most widely used construction material globally [1]), can perfectly constitute its granulometric skeleton.

Millions of tons of electric arc furnace slags (EAFS) are generated annually in the EU. A large part of this by-product still has no application, but after undergoing a recovery process (typically cooling, watering, crushing and screening [2]) it constitutes a high-quality aggregate (siderurgical aggregate) with which it is even possible to manufacture a structural high-performance concrete [3]. Compared with concrete with conventional aggregates (mainly limestone and siliceous material), siderurgical aggregate concrete exhibits a substantial improvement in compressive strength [4–8] and elastic modulus [6,9], mainly due to the higher elastic modulus of SA. The generalized improvement of the mechanical properties has been substantiated by the formation, between aggregate and paste, of a slightly porous interfacial transition zone (ITZ), in which the irregular shape of the aggregates and their high toughness favor a gear effect with the paste [10–12].

* Corresponding author.

E-mail address: thomasc@unican.es (C. Thomas).

<https://doi.org/10.1016/j.job.2022.104595>

Received 2 March 2022; Received in revised form 11 April 2022; Accepted 29 April 2022

Available online 6 May 2022

2352-7102/© 2022 The Authors. Published by Elsevier Ltd. This is an open access article under the CC BY-NC-ND license (<http://creativecommons.org/licenses/by-nc-nd/4.0/>).

The good bond between aggregate and paste in concrete with SA [3,13] would lead to the expectation of good adherence between aggregates and reinforcements (e.g. steel wires or steel bars), however, there are studies on this in the literature on reinforced concrete with SA. The mutual transfer of forces between the reinforcements and concrete is known as adherence and reinforced concrete is based on this. Adherence stresses are influenced by a variety of factors such as geometry, arrangement, corrosion and surface type of the reinforcement, nature of loads, boundary conditions, stresses in surrounding concrete or embedment length [14]. If all the variables that depend on the reinforcements remain constant, bond adhesion will depend above all on the compressive strength of the concrete (since force is transmitted through adhesion, and failure can occur as a result of tensile and shear splitting), composition, consistency (the higher the consistency the higher the adhesion) [15] and the gripping effect of drying shrinkage [16]. If everything in the concrete is maintained constant except the type of aggregate, inevitably the adhesion strength will depend on the characteristics of these particles. A greater roughness of the aggregates will bring about greater friction with the reinforcement and thus greater impediment to the relative displacement between both.

The way to experimentally characterize the adhesion capacity of concrete has traditionally been pullout tests and beam tests. The pullout tests have a series of disadvantages such as the overestimation of the bond capacity of the deformed bars due to friction from the rigid base plate laterally confined by the concrete cylinder [17]. Another disadvantage of these tests is that failure by splitting of the concrete may occur at a load below the maximum bond capacity when ribbed bars are used [18]. The disadvantages of beam tests (e.g. ASTM A944) can be summarized in the difficulty in assembly and the need for a specific experimental setup.

Regarding the quality of the adhesion bond, it should be emphasized that greater porosity of the ITZ with the reinforcement offers a space through which corrosion products can percolate. This corrosion in turn worsens the quality of the ITZ [15], although there are currently coatings (e.g. epoxy) that protect the reinforcements against corrosion [19].

Regarding another critical aspect of concrete, namely durability, recent studies have shown that concrete with these siderurgical aggregates more than fulfills the requirements of permeability to oxygen and water under pressure, offering protection against corrosion of reinforcements and against accelerated carbonation, offering an excellent durability against wear abrasion and resisting the action of freeze-thaw three times more than limestone concrete [20,21].

The present work focuses on the characterization of the adherence strength of concrete with SA, in comparison with a limestone reference concrete. The adherence test consists of measuring the penetration of prestressed steel wires in a beam, while also characterizing the mechanical properties of all concrete mixes. The ITZ of both types of aggregates is also analyzed to establish a relationship with adherence. The study is completed with the analysis of the hardness (in terms of micro-Vickers hardness) of the different concrete mixes, in order to know the bond strength of the pastes that incorporate various amounts of fine SA.

The results obtained will make it possible to establish the suitability of reinforced concrete with siderurgical aggregates, whose use is not currently contemplated in any Spanish regulation, either nationally (Structural Code [22]) or at the regional level within the three autonomous communities that pioneered the use of SA [23–25]. Positive results would open the door to a new application for these sustainable concretes.

2. Materials and methods

2.1. Materials

The EAFS used were cooling treated using water (slow reduction of temperature but enough to fracture the slag and recover the metallic steel) and maintained in water to contain the expansive compounds, after which the slag waste was sieved to produce the siderurgical aggregate. Both natural aggregates (limestone) and siderurgical aggregates were used in different concrete mixes. The natural aggregates (NA) used include the fractions 12/18, 6/12, 0/6 and 0/3 mm, while the siderurgical aggregates (SA) include the fractions 8/16, 4/8, 0/4 and 0/2 mm (this last crushed in laboratory). The particle size distributions can be observed in detail in Fig. 1.

Table 1 shows the main physical-mechanical properties of the aggregates used to obtain the concrete. The properties studied were bulk density, water absorption and porosity (EN 1097–3 and EN 1097–6), sand equivalent (EN 933–8), Los Angeles coefficient (EN 1097–2) and aggregates crushing value (ISO 20290–3). The test fractions used in Los Angeles test include the one proposed by the

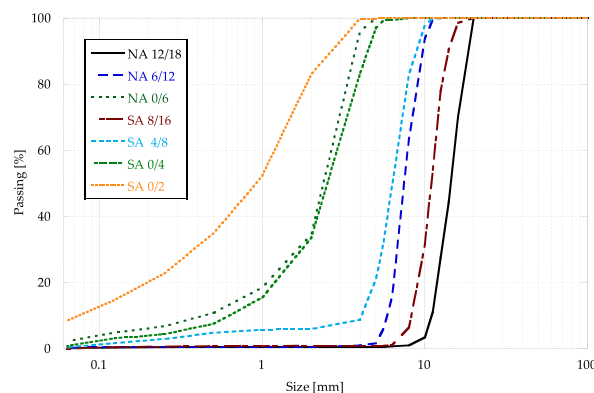


Fig. 1. Particle size distributions of the aggregates used.

Table 1
Physical-mechanical properties of aggregates.

Aggregate	Bulk density (g/cm ³)	Water absorption (% wt.)	Porosity (% vol.)	Sand equivalent (%)	Los Angeles coeff. (%)	Aggregates crushing value (%)
Limestone	2.67	1.50	3.95	77	25	25
Siderurgical	3.83	1.44	6.52	88	17	18

standard as a standard fraction (10–14 mm), complying with the granulometric curve of requirement "A" (60% passing through the 12.5 mm sieve). The test fraction of the sand equivalent test has been 0–2 mm. When comparing siderurgical aggregates to natural aggregates, their 30% higher density coupled with their resistance to wear and crushing stand out.

The main crystalline phases of the siderurgical aggregates were analyzed using a Bruker D8 Advance X-ray diffractometer (Fig. 2). The shape of the bottom envelope (almost straight) shows that the nature of these aggregates is completely crystalline, so chemical reactions with the paste are not expected. Moreover, the main phases exhibited by the samples are iron oxides, mainly wuestite (FeO) and magnetite (Fe₃O₄), although there is also a high presence of magnesioferrite (Fe₂MgO₄). Free magnesia was not detected, so there was no expectation of finding the expansive behavior associated with these siderurgical aggregates [26].

The results obtained by X-ray fluorescence (XRF) using an ARL-ADVANT-XP thermo spectrometer model (Table 2) show a content of iron oxides close to 45%, calcium oxide 22% and silicon oxides around 11%. The iron oxide content is higher than that found in other well-known studies, in which it ranges from 30 to 38% [3,9,27], which has an impact on both the density and the mechanical performance of these aggregates.

2.2. Mix proportions

For this study, three concrete mixes were designed. Dosing was performed using the Fuller method (Fig. 3), setting the amount of CEM, water, superplasticizer additive (SP) and the volume of aggregates, to compare only the effect of replacing aggregates. There are three proposed mix proportions (Table 3):

- LLC: reference concrete that only incorporates limestone aggregates (NA).
- SLC: concrete that incorporates SA in addition to limestone sand, to make up for the lack of fines at source from the crushing plant.
- SSC: concrete that only incorporates siderurgical aggregates, making up for the lack of fines by crushing fine sand from siderurgical aggregate in the laboratory.

The mixing methodology is based on ASTM C192 and consists of a total mixing time of 8 min. During the first 3 min, the aggregates from largest to smallest size, CEM and water were added. For the next 3 min the batch was left to rest and in the last 2 min the mixing was continued with the incorporation of the superplasticizer additive. Concrete compaction was carried out by means of a vibrating needle, while demoulding was carried out 24 h after manufacture and curing in a humidity chamber at 95 ± 5% humidity and at a temperature of 20 ± 2 °C. The manufacturing process of the prestressed beam is described later.

2.3. Concrete mechanical properties

In terms of mechanical properties after 28 days, compressive strength (f_c) was obtained on five cubic specimens (100 mm side) in accordance with EN 12390–3, using a universal servo-hydraulic press with a capacity of 2500 kN and a load application speed of 5 kN/s (0.5 MPa/s).

The secant elastic modulus (E) was calculated using three standard cylindrical specimens (150 × 300 mm) in accordance with EN 12390–13. Method B was used, capping with sulfur on the upper faces of the specimens and fitting them with 120 mm long and 120 Ω

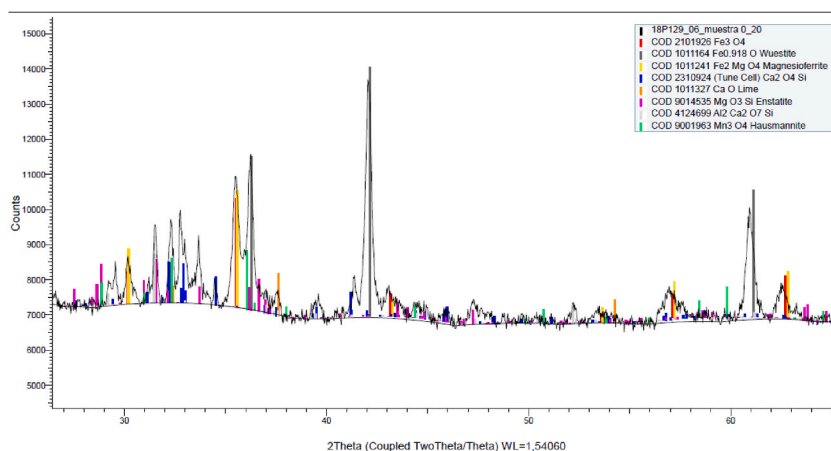


Fig. 2. X-ray diffractogram of the siderurgical aggregates.

Table 2
XRF composition of the SA (% wt.).

Material	SiO ₂	Al ₂ O ₃	Fe ₂ O ₃	MnO	MgO	CaO	Na ₂ O	TiO ₂	P ₂ O ₅	SO ₃	V ₂ O ₅	Cr ₂ O ₃
SA	10.57	6.19	44.79	5.95	7.09	21.99	0.03	0.51	0.29	0.27	0.36	5.53

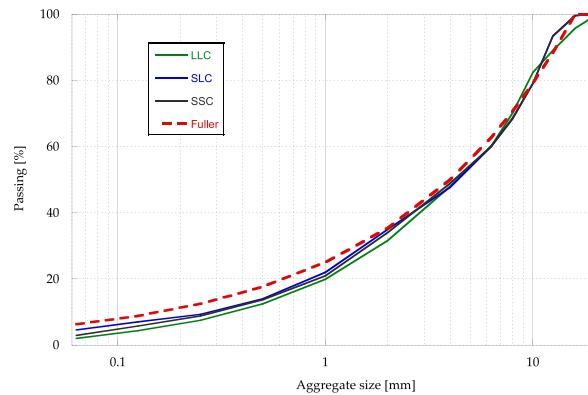


Fig. 3. Grading curves of the combination of aggregates of the different concretes.

Table 3
Proportions of the mixes designed (kg/m³).

Component	LLC	SLC	SSC
CEM I 52.5 R	340	340	340
Effective water	160	160	160
NA 12/20	284	–	–
NA 6/12	662	–	–
NA 0/6	946	776	–
SA 8/16	–	722	722
SA 4/8	–	484	484
SA 0/4	–	443	443
SA 0/2 ^a	–	–	1155
SP	3.4	3.4	3.4
w/c ratio	0.47	0.47	0.47

^a Crushed in the laboratory.

strain gauges. The tests were carried out in a servo-hydraulic press with a capacity of 1000 kN at a load/unload application speed of 8.8 kN/s.

The tensile splitting strength ($f_{t,t}$) of three standard cylindrical specimens (150 × 300 mm) was evaluated using a universal servo-hydraulic press with a capacity of 2500 kN and a load application speed of 3.5 kN/s in accordance with EN 12390–6.

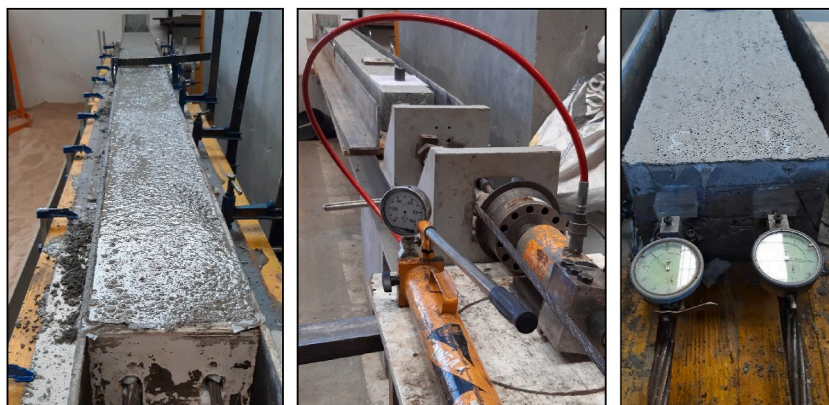


Fig. 4. Formwork filling, demoulding and slacking of the steel wires, and penetration measurement.

The flexural strength (σ) of five prismatic specimens ($100 \times 100 \times 400$ mm) was obtained according to EN 12390-5, with the variant of using a single centered load roller (supported in three points). To carry out the tests, a load application speed of 109 N/s and a universal servo-hydraulic press with a capacity of 250 kN were used.

2.4. Adherence of prestressed reinforcements

The tests were carried out following the methodology proposed by the UNE 7-436-82: test method for determining the adherence characteristics of prestressing reinforcements, for which the LADICIM laboratory is accredited by the ILAC. Beams were manufactured with both LLC and SSC mixes. Two 15.2 mm diameter steel wires were used, designated Y 1860 S7, with tensile strength of 1860 MPa. The concrete specimen has dimensions of 3540 mm in length and a section of 200×141 mm² (base x height). Fig. 4 shows, in detail, the formwork and fasteners used to manufacture the reinforced concrete beam.

Once the test load (208 kN) was reached, the corresponding strain gauge strain value is recorded. The first of the wedges is anchored, and the second is released to loosen the jack and remove the load cell. If in the process of removing the cell, the deformation in the reinforcement decreased, the jack was placed again, without a cell, and the reinforcement was reloaded until the deformation was reached again. The tensioning was carried out 24 h before mixing the concrete.

The concrete was manufactured according to the above-mentioned specifications, making batches of 100 l and manufacturing three cubic specimens of 100 mm to check the compressive strength. The vibrating of the beam was carried out similarly, inserting the vibrating needle every 0.5 m. The formwork was removed 24 h after manufacture, at which time the comparators were mounted (precision of 0.01 mm), the initial deformation reading was taken, and the comparator was zeroed; however, the slackening of the armor (Fig. 4) was not performed until the concrete had reached 24.5 MPa (for steels with normal adhesion), testing the cubic specimens to check the compressive strength.

The measurements of this test consist of determining, at the ends of the specimens, the penetration δ (mm) of each of the elements of the active reinforcement, from the penetration reading measured by the comparator (l_m) and the elastic shortening of the reinforcement at the moment of transmission of the prestress (Δa) obtained from Hooke's law. The elastic shortening depends on the load (P), the distance (a), the elastic modulus of the steel wire (E_S) and its area (A_{pn}).

$$\Delta a = \frac{P \cdot a}{E_S \cdot A_{pn}} \quad (1)$$

$$\delta = l_m - \Delta a \quad (2)$$

Five measurements were carried out that made it possible to obtain the penetration of the reinforcement at five different times, before releasing the prestressing and at 1 h, 6 h, 24 h and 7 days after releasing the prestressing. With the mean of the penetrations of all the reinforcements at 7 days (δ_m), the anchor length (L_S) was calculated. The anchor length depends on the maximum stress of the reinforcement ($f_{pm,G}$), the elastic modulus of the reinforcement (E_S) and the area of the reinforcement:

$$L_S = \frac{3.5 \cdot E_S \cdot A_{pn}}{f_{pm,G}} \quad (3)$$

The anchor length and the penetration of the reinforcement in the beam of the two mixes were compared and it was verified that both mixes met the requirements imposed by the standard EHE-08 [28]:

- Anchor length $L_S \leq 0.5L - 150$ mm.
- Reinforcement penetrations, measured during the test, tend to stabilize (value at 24 h ≥ 0.9 of the value at seven days).
- The dispersion S_δ of the reinforcement penetration is less than 30%.
- There is no cracking on the concrete surface during the test.

2.5. Microstructural analysis

An analysis was carried out by means of a scanning electron microscopy (SEM) of the capacity of the paste by studying the paste-aggregate interface (ITZ). A variable pressure Carl Zeiss EVO MA15 SEM equipped with an Oxford Instruments X-ray detector was used. This SEM operates under low vacuum conditions, using a lanthanum hexaboride filament as a source of electrons, being able to detect backscattered electrons in addition to being able to determine the elemental composition by means of an EDX detector.

The ITZ is the most important interface in concrete and the one responsible for mechanically characterizing its response [29]. For this reason, this transition zone is the area of greatest weakness of the material. The adhesion between paste and aggregate is an unequivocal indication of the possible paste-reinforcement adherence, since the mechanisms that reinforce this union are the same, and they depend on the mechanical characteristics of the aggregates as well as on their geometry. The samples used were extracted from the center of cylindrical specimens and were duly polished.

In addition, micrographs of the aggregates and the cement paste were obtained separately using the same samples, to identify the differences between the different mix proportions or the difference between using a conventional aggregate or a siderurgical aggregate.

2.6. Micro vickers hardness test

The LLC, SLC and SSC subsamples were stuffed using an epoxy system consisting of a resin and a hardener, pouring this compound into cylindrical polypropylene molds of 3 cm in diameter and 2 cm in height. The mixture was allowed to cure at room temperature for

24 h and before removing from the mold and polishing. During the polishing process, abrasive discs were used in decreasing order of grain size, using discs with 320, 500, 1000, 2000 and 4000 (FEPA) grit sizes. An electric polisher was used at 30 rpm and an applied load of 30 N. The process carried out to obtain the polished specimens is outlined in Fig. 5.

A Neurtek brand Vickers micro-durometer was used to measure hardness, which incorporates a load cell, automatic sample recognition, automatic image analysis and an optical microscope. The measurement of the hardness of the concrete cement paste was performed by means of 5 measurements, applying a load (F) of 0.05 N and measuring the diagonals of the mark left by the penetrator (d), which in this case is a diamond pyramid. The indentation was made in areas of paste. The Vickers hardness (HV) can be obtained through the mean value of the diagonals of the indentation and the applied force using the following expression:

$$HV = \frac{1.8544 \cdot F}{d^2}$$

3. Results and discussion

3.1. Concrete mechanical properties

The main factors that affect adherence are the tensile strength of the concrete layer underneath the externally applied composite, the roughness and cleanliness of the face in contact with the reinforcement [30], and the elastic modulus of the concrete. This is why it is necessary to quantify the mechanical properties of concrete when studying its adherence properties.

Table 4 shows the mechanical properties of the mixes produced. The SLC and SSC mixes show a compressive strength 42% and 75% higher than the LLC mix, respectively. These differences are reduced for the elastic modulus and for the tensile splitting strength, where the role of the paste is more decisive than that of the aggregates. In flexural strength, the effect of total replacement is remarkable, the higher mechanical performance always corresponding to the use of siderurgical aggregates, which are more resistant and make an improved ITZ, as will be shown later.

Fig. 6 shows the appearance of specimens subjected to the tensile splitting strength (Fig. 6 left) and flexural strength (Fig. 6 right) tests. Having paste of lower density than the coarse aggregate can facilitate segregation towards the bottom of the specimens, however, a correct distribution of the aggregates is observed, even in the case of the SLC mix, which incorporates limestone sand. The cracking of the specimens occurred through the aggregates, showing a good bond in the ITZ between paste and aggregates.

3.2. Adherence of prestressing reinforcements

As shown in the methodology of this test, a measurement of the penetration of two reinforcements is made on both sides of a concrete beam with standardized dimensions. Fig. 7 shows the comparator measurements at each of the four points where the reinforcement penetrates the concrete beam. Measurements have been made at 1, 6, 24 h and 7 days.

The bond between the reinforcing bar and the surrounding concrete depends on the quality of the paste because there are no coarse aggregates in the thin bond layer. The quality of the paste in turn depends on two main aspects, the first is that there is a sufficient quantity of fine particles, and the second is that the shape and characteristics of these particles favor a high gear effect. Table 5 shows



Fig. 5. Sample preparation and placement in the optical microscope.

Table 4
Mechanical properties of the mixes produced.

Mix	f_c (MPa)	E (GPa)	f_{ct} (MPa)	σ (MPa)
LLC	62.90 ± 6.22	41.25 ± 0.31	3.54 ± 0.19	9.47 ± 0.10
SLC	89.45 ± 3.15	53.48 ± 1.05	4.12 ± 0.16	9.97 ± 0.22
SSC	110.39 ± 0.82	58.61 ± 0.64	4.79 ± 0.32	12.92 ± 0.25

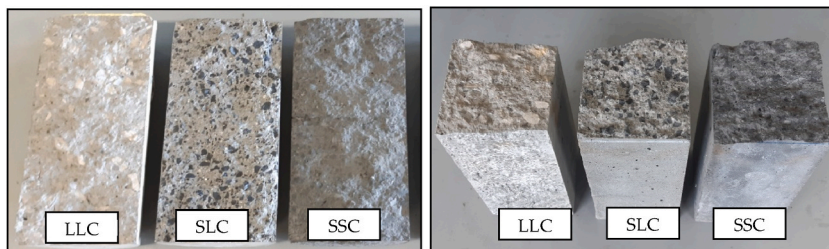


Fig. 6. Appearance of the specimens after tensile splitting strength (left) and flexural strength tests.

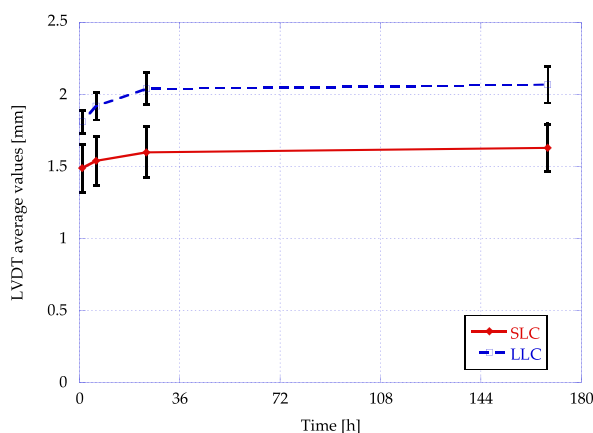


Fig. 7. Evolution of the average reading of the LVDT.

the results obtained in the adherence test. The penetration of the reinforcement in the concrete (δ) for the SLC mix is 23% lower, which shows that the siderurgical aggregate provides better steel reinforcement adherence. The fines (<0.063 mm) content is similar in both concrete mixes (about ~5%) so this higher adherence strength is explained by the great roughness and the irregular shape of the siderurgical aggregates, which favors the concrete-reinforcement bond. The dispersion of the reinforcement penetrations is much lower in the SLC mix, while the anchorage length (straight length for anchoring the force) is also 23% lower for this mix.

To validate these test results, some demanding requirements must be satisfied, which are shown in Table 6. Both the LLC and the SLC mixes easily exceed each of the requirements, although the SLC mix exceeds them more comfortably. In addition, none of the mixes showed a surface break in the concrete during the test (Fig. 8), so the tests had satisfactory results.

3.3. Microanalysis

Micrographs with a high magnification (1500 X) were used for the analysis of the surface of the aggregates. Fig. 9 (left) and Fig. 9 (right) show the surface of the limestone and siderurgical aggregates respectively. The limestone aggregate has a smaller number of pores; however, their size seems to be greater than that of the siderurgical aggregate. The siderurgical aggregate, on the contrary, shows a homogeneous network of small pores generated during the slow cooling process of the slags. The polishing of the samples does

Table 5
Adherence test results.

Variable	SLC	LLC
δ (mm)	1.23	1.60
S δ (%)	16	29
Ls (mm)	487.03 ± 61.36	633.74 ± 116.73

Table 6
Requirements to validate the adherence test.

Requisites	LLC		SLC	
$L_s \leq 0.5 L-150$	633.7	≤ 1620	487.0	≤ 1620
$L_{m24hLVDT1} \geq 0.9 \cdot L_{m7dLVDT1} =$	2.03	≥ 1.79	1.50	≥ 1.36
$L_{m24hLVDT2} \geq 0.9 \cdot L_{m7dLVDT2} =$	1.92	≥ 1.82	2.12	≥ 1.91
$L_{m24hLVDT3} \geq 0.9 \cdot L_{m7dLVDT3} =$	2.35	≥ 2.19	1.38	≥ 1.29
$L_{m24hLVDT4} \geq 0.9 \cdot L_{m7dLVDT4} =$	1.85	≥ 1.66	1.40	≥ 1.30
$S_{\delta} < 0.3 \cdot \delta_m =$	0.29	0.49	0.16	≤ 0.37
Cracking on the concrete surface:	No		No	



Fig. 8. Surface of the SLC mix beam.

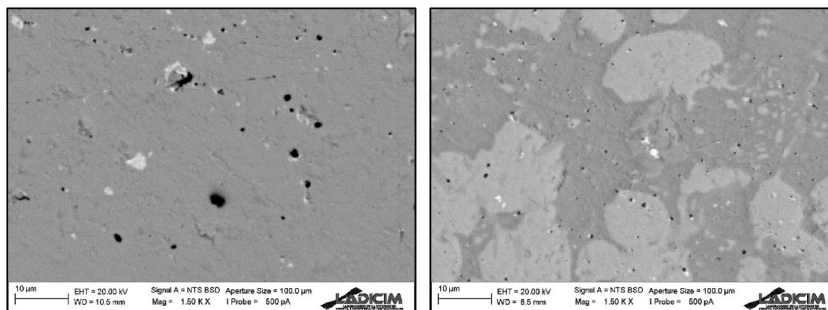


Fig. 9. Micrograph of limestone aggregate (left) and siderurgical aggregate (right) at 1500 X.

not allow a comparison of the topography of the aggregates, however, in the siderurgical aggregate there are two phases, the whitish more dense one showing agglomerations in the form of iron oxides (wuestite and magnetite) in a solid solution with other metals such as Si, Ca or Mg.

In Fig. 10 (left), a 500x magnification micrograph of the LLC paste, a certain degree of homogeneity can be observed in the paste, as well as a homogeneous distribution of the microporosity, which is defined by the holes (black dots) that appear on the surface of the paste. The size of these holes/pores does not exceed 10 μm (maximum length measured by a tool of the SEM) in any case and a good union within the paste is observed. The micrograph shows a good quality calcium-silicate-hydrate (CSH) gel, maintaining an amorphous structure without discontinuities or apparent capillaries.

In the micrograph of the SLC paste at 500 X magnification, Fig. 10 (right), corresponding to the SLC mix, a homogeneous distribution of the micropores within the paste, which is porous by nature [31] is also observed. It can also be seen that the size of these micropores is similar to that of the previous micrograph and they are never greater than 10 μm. The network of pores is similar and is due to the amorphous nature of the CSH gel, although in this micrograph the image is less distorted than that of the LLC mix (Fig. 10 left) due to the iron nature of the paste itself (more conductive). The good condition of the paste (compact paste, without alterations, discontinuities or large pores) and the darker tonality of the micrograph due to the difference in density between aggregates and paste should be noted. No large microstructural differences are observed at the pore/capillary level, which shows a similar spatial distribution of particles in both mix proportions.

Fig. 11 (left) and Fig. 11 (right) show the micrographs obtained for the LLC mix at 150 and 500 X magnifications respectively. Aggregates can be distinguished, with a less rough shape and a more homogeneous texture than paste, which has a more porous and less homogeneous structure. Likewise, a similar tonality is observed for both phases, which shows a similar density between paste and

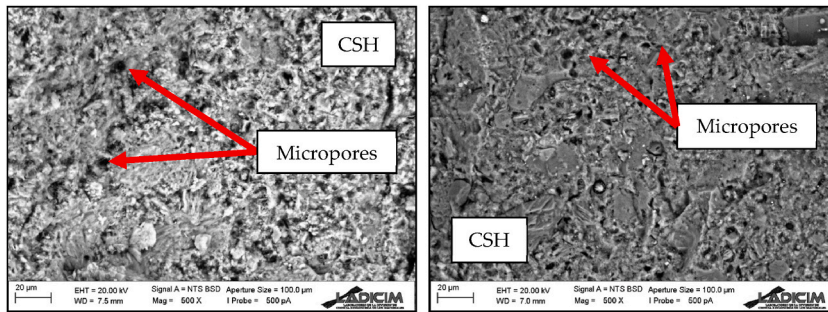


Fig. 10. Micrograph of the paste of the LLC mix (left) and SLC mix (right) at 500 X.

aggregates.

The ITZ corresponds to a thickness of about 20 μm around the aggregate (similar to the average size of a CEM grain) [32]. This interface can compromise the mechanical properties of concrete because it constitutes the area of greatest weakness. In the interface shown in Fig. 11 (right), shades of different brightness are not observed, which shows that there is no presence of unhydrated cement grains. Likewise, it is observed that the border area between both phases is porous, implying that the joint area is not perfectly covered by the paste. This porous zone can be the main penetration route for chemically aggressive ions [32,33], so the micrographs can provide an idea of the durability of the different mixes in addition to their mechanical capacity. One way to reduce the porosity of the ITZ would consist of the incorporation of fillers [34] such as silica fume, particles that fill the gaps and favor a more homogeneous distribution of stress.

Fig. 12 (left) and Fig. 12 (right) show in detail the paste-aggregate ITZ for the SSC mix, where the SA is covered by the cement paste. In both micrographs, and in more detail in the micrograph at 500 X magnification, a more compact ITZ can be observed, better filled by the paste than for the LLC mix. The paste-aggregate interface is less porous and therefore more homogeneous, establishing the porosity as the space shown in the interface or border, with a greater space or gap in the case of natural aggregate. This lower porosity explains the greater mechanical behavior in the mix using siderurgical aggregate. The paste containing siderurgical aggregate is capable of adhering more to the surface of the siderurgical aggregate, which has a high tenacity, so that the siderurgical aggregate has a superior gear capacity, which would also be expected to be greater at the interface with the active reinforcements.

On the other hand, the surrounding cementitious matrix does not show the presence of non-hydrated cement grains and the continuity of this transition zone is such that a certain width of the porous discontinuity cannot be established, as happens in the case of LLC. This is approximately 2 μm on average around its entire contour.

3.4. Micro vickers hardness

In Fig. 13, some of the traces of the micro-indenter produced in the pastes obtained with an optical microscope using a 40 X magnification are shown, which were made far enough away from the aggregates to avoid their influence on this property [27].

A higher hardness value corresponds to a lower value of the diagonal of the indenter imprint. It can be observed that, in all the tests carried out, the stamped trace can be clearly discerned, so the selected value of test load (0.5 N) is adequate. Moreover, note that the color of the paste turns whitish for LLC concrete, and for SLC concrete, black specks appear caused by the color of the fine aggregates of the siderurgical aggregates. In the case of the SSC concrete, whose fines content corresponds entirely to sand from siderurgical aggregates, a much darker color of the paste is observed. A greater ease of reading was possible for the LLC and SLC mix, since the selected load allows good printing as well as the visualization of each of the indenter edges.

The results obtained individually enabled the average Vickers hardness values to be obtained for each concrete, represented in Fig. 14 (left) together with their standard deviation (whiskers). It can be seen that the incorporation of a greater volume of siderurgical aggregate fines in the cement paste corresponds to a greater hardness. SSC concrete shows greater hardness than the rest, on the one

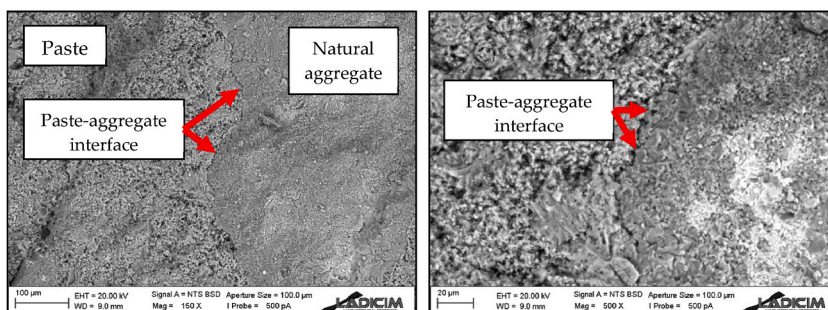


Fig. 11. Micrograph of the ITZ of LLC mix at 150 X (left) and 500 X (right).

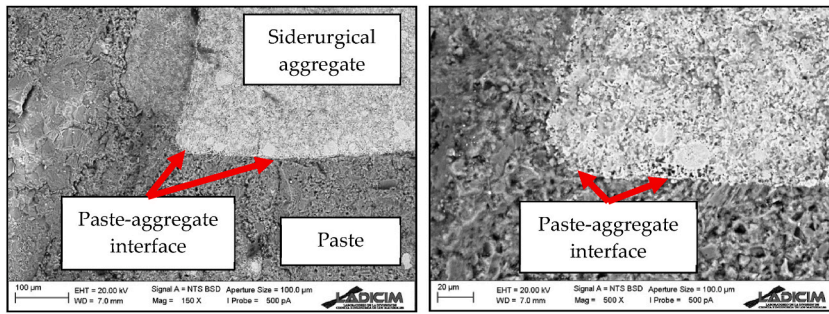


Fig. 12. Micrograph of the ITZ of SLC mix at 150 X (left) and 500 X (right).

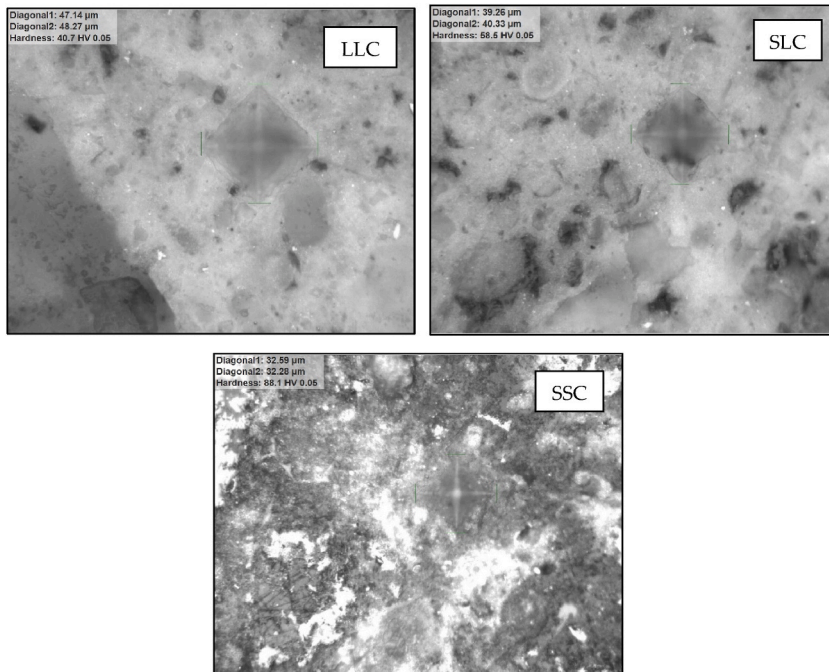


Fig. 13. Images of the stamped traces obtained for LLC, SLC and SSC mix.

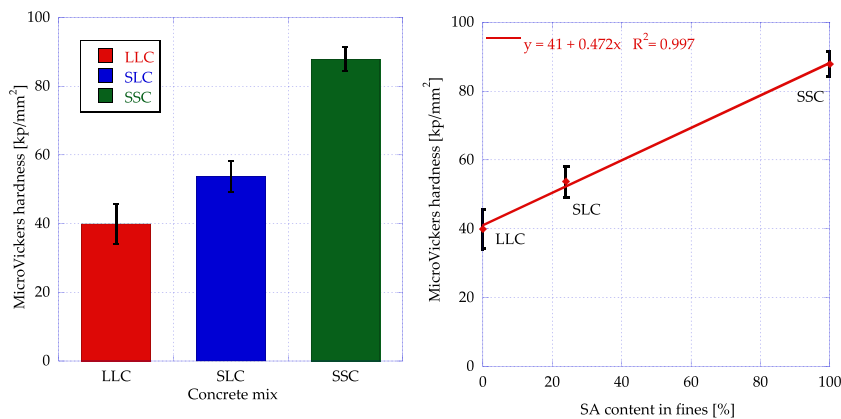


Fig. 14. MicroVickers hardness (left) and influence of the SA content in fines (right).

hand, the hardness of the siderurgical aggregate is higher than that of the limestone aggregate, but a higher level of adherence between the cement and the fines helps to increase this value. This effect is also observed for the SLC mix, where a small content of fine siderurgical aggregates shows a substantial increase in hardness. In relative terms, the hardness of LLC concrete is almost 30% lower than SLC and 55% lower than SSC. These values show a high level of surface cohesion of the particles, which, as shown in Fig. 14 (right), depends directly on the fines content of fine siderurgical aggregates (<4 mm), showing a proportional relationship with an excellent fit ($R^2 \sim 1$).

4. Conclusions

In this work, the adherence strength of prestressed concrete with both siderurgical and limestone type aggregates is analyzed. The results obtained are explained through the study of the ITZs of both types of aggregate with the paste. The bonding strength between aggregate and paste is established by means of Vickers micro-hardness tests. After analyzing the results obtained, the following conclusions can be drawn:

- The penetration of the prestressed reinforcement is 23% lower for the SLC mix than for the LLC mix, which shows better concrete-reinforcement bonding with the siderurgical aggregate due to its roughness and irregular shape. This means that the necessary anchor length is 23% less for the SLC mix.
- The paste-aggregate interface (ITZ) of concrete with siderurgical aggregates is less porous than with limestone aggregates, which indicates better grinding effect between them as well as better adherence with steel reinforcements due to the shape and nature of the siderurgical aggregate.
- The hardness of the concrete pastes increases proportionally with the degree of replacement of the fines by siderurgical aggregate. For total replacement values (SSC mix), the hardness of the pastes is 55% higher than that of the limestone reference concrete (LLC).
- Current regulations do not contemplate the use of siderurgical aggregates in the manufacture of reinforced concrete, but the properties of the experimental campaign carried out suggest that it is an ideal application for these sustainable concretes.

Credit author roles

Conceptualization: Tamayo, P.; Polanco, J.A.; Thomas, C.; Data curation: Tamayo, P.; Aghajanian, A.; Thomas, C. Formal analysis: Tamayo, P.; Aghajanian, A.; Thomas, C.; Funding acquisition: Thomas, C.; Polanco, J.A.; Project administration: Thomas, C.; Polanco, J.A.; Resources: Thomas, C.; Polanco, J.A.; Supervision: Thomas, C.; Polanco, J.A.; Validation: Tamayo, P.; Aghajanian, A.; Rico, J.; Setién, J.; Polanco, J.A.; Thomas, C. Visualization: Thomas, C.; Polanco, J.A.; Writing - original draft: Tamayo, P.; Thomas, C. Writing - review & editing Tamayo, P.; Rico, J.; Polanco, J.A.; Thomas, C.

Declaration of competing interest

The authors declare that they have no known competing financial interests or personal relationships that could have appeared to influence the work reported in this paper.

Acknowledgments

This research was co-financed by the European Regional Development Fund (ERDF) and the Ministry of Economy, Industry and Competitiveness (MINECO) within the framework of the project RTC-2016-5637-3. The research was possible thanks to the collaboration of the company INGECID, the department LADICIM (University of Cantabria) and the companies ROCACERO and SIDENOR, as well as the Department of Universities and Research, Environment and Social Policy of the Government of Cantabria (Spain).

References

- [1] T. Wangler, E. Lloret, L. Reiter, N. Hack, F. Gramazio, M. Kohler, M. Bernhard, B. Dillenburger, J. Buchli, N. Roussel, others, Digital concrete: opportunities and challenges, *RILEM Tech. Lett.* 1 (2016) 67–75.
- [2] C. Thomas, J. Rosales, J.A. Polanco, F. Agrela, 7 - steel slags, in: J. de Brito, F. Agrela (Eds.), *New Trends Eco-Efficient Recycl. Concr.*, Woodhead Publishing, 2019, pp. 169–190, <https://doi.org/10.1016/B978-0-08-102480-5.00007-5>.
- [3] I. Sosa, C. Thomas, J.A. Polanco, J. Setién, P. Tamayo, High performance self-compacting concrete with electric arc furnace slag aggregate and cupola slag powder, *Appl. Sci.* 10 (2020) 773.
- [4] N.H. Roslan, M. Ismail, Z. Abdul-Majid, S. Ghoreishiamiri, B. Muhammad, Performance of steel slag and steel sludge in concrete, *Construct. Build. Mater.* 104 (2016) 16–24, <https://doi.org/10.1016/j.conbuildmat.2015.12.008>.
- [5] P.O. Awoyera, A.W. Adekeye, O.E. Babalola, Influence of electric arc furnace (EAF) slag aggregate sizes on the workability and durability of concrete, *Int. J. Eng. Technol.* 7 (2015) 1049–1056.
- [6] M. Maslehuddin, A.M. Sharif, M. Shameem, M. Ibrahim, M.S. Barry, Comparison of properties of steel slag and crushed limestone aggregate concretes, *Construct. Build. Mater.* 17 (2003) 105–112.
- [7] A.S. Brand, J.R. Roesler, Steel furnace slag aggregate expansion and hardened concrete properties, *Cement Concr. Compos.* 60 (2015) 1–9, <https://doi.org/10.1016/j.cemconcomp.2015.04.006>.
- [8] C. Pellegrino, P. Cavagnis, F. Faleschini, K. Brunelli, Properties of concretes with black/oxidizing electric arc furnace slag aggregate, *Cement Concr. Compos.* 37 (2013) 232–240, <https://doi.org/10.1016/j.cemconcomp.2012.09.001>.
- [9] S. Monosi, M.L. Ruello, D. Sani, Electric arc furnace slag as natural aggregate replacement in concrete production, *Cement Concr. Compos.* 66 (2016) 66–72, <https://doi.org/10.1016/j.cemconcomp.2015.10.004>.
- [10] P. Tamayo, J. Pacheco, C. Thomas, J. de Brito, J. Rico, Mechanical and durability properties of concrete with coarse recycled aggregate produced with electric arc furnace slag concrete, *Appl. Sci.* 10 (2020) 216.
- [11] P. Tamayo, C. Thomas, J. Rico, J. Setién, J.A. Polanco, S. Pérez, S. Mañanes, Radiological shielding concrete using steel slags, in: *Waste Byprod. Cem. Mater.*, Elsevier, 2021, pp. 413–438.

- [12] A.S. Brand, J.R. Roesler, Interfacial transition zone of cement composites with steel furnace slag aggregates, *Cement Concr. Compos.* 86 (2018) 117–129, <https://doi.org/10.1016/j.cemconcomp.2017.11.012>.
- [13] I. Papayianni, E. Anastasiou, Utilization of electric arc furnace steel slags in concrete products, *Ferr. Slag-Resource Dev. an Environ. Sustain. World.* (2010) 319–334.
- [14] A. Wojtowicz, A. Ubysz, J. Michałek, How vibrations affect steel-to-concrete adherence, in: *MATEC Web Conf.*, 2018, p. 2045.
- [15] A. Tamrazyan, Problems of Modelling the Bond Reinforcement in Concrete, *E3S Web Conf.*, 2021.
- [16] S.M. Dewi, A. Soehardjono, The Comparison between Pull-Out Test and Beam Bending Test to the Bond Strength of Bamboo Reinforcement in Light Weight Concrete, 2013.
- [17] G. Xing, C. Zhou, T. Wu, B. Liu, Experimental study on bond behavior between plain reinforcing bars and concrete, *Adv. Mater. Sci. Eng.* 2015 (2015).
- [18] O. Kayali, S.R. Yeomans, Bond of ribbed galvanized reinforcing steel in concrete, *Cement Concr. Compos.* 22 (2000) 459–467.
- [19] J. Lee, E. Sheesley, Y. Jing, Y. Xi, K. Willam, The effect of heating and cooling on the bond strength between concrete and steel reinforcement bars with and without epoxy coating, *Construct. Build. Mater.* 177 (2018) 230–236.
- [20] J.A. Sosa, I. P. Tamayo, J.A. Sainz-Aja, C.* Thomas, J. Setién, I. Sosa Polanco, P. Tamayo, J.A. Sainz-Aja, C. Thomas, J. Setién, J.A. Polanco, Durability aspects in self-compacting siderurgical aggregate concrete, *J. Build. Eng.* 39 (2021), <https://doi.org/10.1016/j.job.2021.102268>.
- [21] I. Sosa, C. Thomas, J.A. Polanco, J. Setién, J.A. Sainz-Aja, P. Tamayo, Durability of high-performance self-compacted concrete using electric arc furnace slag aggregate and cupola slag powder, *Cement Concr. Compos.* (2022), 104399, <https://doi.org/10.1016/j.cemconcomp.2021.104399>.
- [22] M. de Fomento - Gobierno de España, Structural Code, 2019.
- [23] C. autónoma del Pa, Vasco, Decreto 64/2019: Regimen jurídico aplicable a las actividades de valorización de escorias negras procedentes de la fabricación de acero en hornos de arco eléctrico, in: *Ico, BOPV*, 2019.
- [24] D.O. de, la G. de Catalunya, Decret 32/2009, de 24 de febrero, Valorització d'escòries siderúrgiques de Catalunya., 2009.
- [25] C. de gobierno de Cantabria, Decree 100/2018: Valorización de escorias en la Comunidad Autónoma de Cantabrie, *BOC*, 2018.
- [26] V. Ortega-López, J.A. Fuente-Alonso, A. Santamaría, J.T. San-José, Á. Aragón, Durability studies on fiber-reinforced EAF slag concrete for pavements, *Construct. Build. Mater.* 163 (2018) 471–481, <https://doi.org/10.1016/j.conbuildmat.2017.12.121>.
- [27] I. Arribas, A. Santamaría, E. Ruiz, V. Ortega-López, J.M. Manso, Electric arc furnace slag and its use in hydraulic concrete, *Construct. Build. Mater.* 90 (2015) 68–79, <https://doi.org/10.1016/j.conbuildmat.2015.05.003>.
- [28] M. de Fomento - Gobierno de España, EHE-08: Code on Structural Concrete, 2008. http://www.fomento.gob.es/MFOM/LANG_CASTELLANO/ORGANOS_COLEGIADOS/CPH/instrucciones/EHE08SINGLES/.
- [29] K.L. Scrivener, A.K. Crumbie, P. Laugesen, The interfacial transition zone (ITZ) between cement paste and aggregate in concrete, *Interface Sci.* 12 (2004) 411–421.
- [30] G. Galecki, N. Maerz, A. Nanni, J. Myers, Concrete substrate preparation with waterjets for repair and strengthening of concrete, in: *7th Pacific Rim Int. Conf. Water Jet, Technol.*, 2003, pp. 245–255.
- [31] S. Bahafid, S. Ghabezloo, M. Duc, P. Faure, J. Sulem, Effect of the hydration temperature on the microstructure of Class G cement: CSH composition and density, *Cement Concr. Res.* 95 (2017) 270–281.
- [32] J.P. Ollivier, J.C. Maso, B. Bourdette, Interfacial transition zone in concrete, *Adv. Cement Base Mater.* 2 (1995) 30–38.
- [33] K.A. Snyder, D.P. Bentz, E.J. Garboczi, 27 INTERFACIAL ZONE PERCOLATION IN CEMENT-AGGREGATE COMPOSITES, *interfaces cem, Composer* (1992) 259.
- [34] A. Goldman, A. Bentur, Effects of pozzolanic and non-reactive microfillers on the transition zone in high strength concretes, in: *RILEM Proc*, 1992, p. 53.